Journal of the European Ceramic Society 21 (2001) 959–968

www.elsevier.com/locate/jeurceramsoc

SiCN nanocomposite: creep behaviour

J-L. Besson [a,*], B. Doucey [b], S. Lucas [b], D. Bahloul-Hourlier [b], P. Goursat [b]

[a] *SPCTS, ENSCI, 47 Av. A. Thomas, 87065 Limoges, France*
[b] *SPCTS, Université de Limoges, 123 Av. A. Thomas, 87060 Limoges, France*

Received 6 July 2000; received in revised form 27 September 2000; accepted 11 October 2000

Abstract

The compressive creep behaviour of a Si_3N_4/SiC nanocomposite densified with yttria and alumina is studied in the 1150–1350°C temperature range under stresses from 45 to 180 MPa. The stress exponent equals 1 and the apparent activation enthalpy is 580 kJ mol^{-1}. Grain boundary sliding accommodated by diffusion through the intergranular glass phase is considered as the primary steady-state creep mechanism. It is argued that the diffusion step through the glass phase is the rate limiting step in the dissolution–diffusion–reprecipitation process. The results are compared with those obtained in previous studies for an α-Si_3N_4 rich monolith and a Si_3N_4/SiC micro-nanocomposite. The high creep deformation is explained by the nanometric size of the Si_3N_4 grains and the absence of grain growth in the temperature range explored. It is showed that a post-sintering heat-treatment consisting in 5 h at 1750°C followed by 3 h at 1400°C enhances the creep resistance to a fair level. It is concluded that the high ductility of the as-sintered material is suitable for hot-forging whereas the subsequent heat-treatment is able to provide shaped parts with a high creep resistance for structural applications at high temperature.

Keywords: Creep; Nanocomposite; Si_3N_4; Si_3N_4/SiC

1. Introduction

The ability of silicon nitride based ceramics to be shaped by hot forging could be advantageous in making parts with complex shapes. Nevertheless, for high temperature applications, these parts, (such as rotor blades for instance), must have a high creep resistance in service at temperature higher than that allowed by metallic superalloys. Since superplastic forming of a Si_3N_4/SiC composite was demonstrated by Wakai and coworkers,[1] a lot of work has been done on superplastic behaviour of different grades of silicon nitrides.[2–14] In this context, it was showed in our laboratory[6,9] that an α-Si_3N_4 rich ceramic could be plastically deformed up to 85% elongation in tension. However, during the deformation, a strong hardening appeared that was attributed to the α-Si_3N_4 equiaxed grains transforming into β-Si_3N_4 elongated grains. To avoid this change in microstructure, it was attempted to hinder the acicular grain growth by incorporating SiC nanoparticles in the Si_3N_4 ceramic. This resulted in a creep resistant micro-nanocomposite with a elongation in tension limited to 39% at 1595°C under a strain rate as low as 10^{-5} s^{-1}.

In the present study, the ductility of a Si_3N_4/SiC composite with a nanosized equiaxed microstructure is compared to the behaviour of the two grades mentioned above. Creep behaviour under compressive solicitation was selected for this first assessment of the ductility for it requires only small samples with a simple geometry.

2. Materials and testing

2.1. Materials

The composite was fabricated by adding to a nanosized SiCN powder, used as the source for Si_3N_4 and SiC, 6 wt.% yttria and 3 wt.% alumina as sintering aids. The nanosized SiCN powder was synthesised by laser pyrolysis[15,16] of a mixture of SiH_4, CH_3NH_2 and NH_3 gases in the respective 50:10:40 volume proportions. The elemental analysis of the SiCN powder is given in Table 1. The SiCN powder consisted in particles of irregular shape associated in hard aggregates. Each

* Corresponding author. Tel.: +33-55545-2222; fax: +33-55579-0998.

E-mail address: jl.besson@ensci.fr (J.-L. Besson).

0955-2219/01/$ - see front matter
PII: S0955-2219(00)00286-7

particle contained α-Si_3N_4 and β-Si_3N_4 crystals and was covered by an amorphous silicon oxycarbonitride phase ($SiO_xC_yN_z$). No free carbon was detected in the powder. The ratio between α-Si_3N_4 and β-Si_3N_4 in the powder was about 50/50.

To achieve a final density close to the theoretical density, the sintering aids needed to be ultrafine powders. Yttria was obtained from Rhône-Poulenc and alumina from Marketec International. Their characteristics are given in Table 2.

The mixing of the powders was done in ethanol and two stages of sonification (Vibra cell 72412, Bioblock Scientific) were introduced to break the hard agglomerates. The slip was homogenised in a polyethylene jar with Si_3N_4 balls to avoid contamination. After drying, the powder was crushed in a mortar and heated under vacuum to eliminate residual ethanol that can be a source for oxygen and free carbon. The flow chart for the process is given in Fig. 1.

The densification schedule was established taking into account studies on the thermal stability of the SiCN powder.[17] The powder mixture was introduced in a graphite die ($\Phi = 30$ mm) lined with high purity boron nitride powder. A 35 MPa pressure was applied to the cold compact and released. The hot-pressing cycle consisted in four temperature steps: 5 min at 1300°C, 20 min at 1450°C, 1 h at 1600°C and 5 min at 1700°C. The first step was conducted under vacuum to allow the residual gases to release before a nitrogen flow be established to avoid decomposition of silicon carbonitride. The initial pressure on the sample was 15 MPa and it was increased to 35 MPa at 1450°C, temperature at which the liquid eutectic appeared, in order to enhance grain rearrangement.

After sintering, the samples were nearly fully dense (99%) and the initial α-Si_3N_4 crystals were fully converted to β-Si_3N_4. The elemental analysis of the sintered bodies is given in Table 3.

Microstructures were examined in a plane perpendicular to the pressing direction by scanning electron microscopy (SEM, JEOL JSM 35) after plasma-etching ($CF_4 + O_2$) and by transmission electron microscopy (TEM, JEOL 2010). The surfaces were coated with a Au–Pd alloy to avoid charge effects during the observations.

The microstructure of the SiCN composite (Fig. 2) was homogeneous and consisted in very fine equiaxed or slightly elongated grains of β-Si_3N_4 (in fact, the β-$Si_{6-x}Al_xO_xN_{8-x}$ solid solution, but with a very low x due to the low alumina addition) embedded in an intergranular YSiAlON glassy phase (Fig. 2b). The mean grain size was ~ 150 nm with the more elongated grains never in excess of 450 nm (Fig. 2a and b). Yttrium was entirely concentrated in the intergranular amorphous phase that, due to the high atomic number of yttrium, was highly electron absorbing and, hence, was always visible in darker contrast than the Si_3N_4 grains. The amorphous phase formed continuous intergranular thin films and pockets at multi-grain junctions (Fig. 2d). The SiC nanoparticles were spherical with sizes less than 30 nm. The precipitates were disseminated either in or in

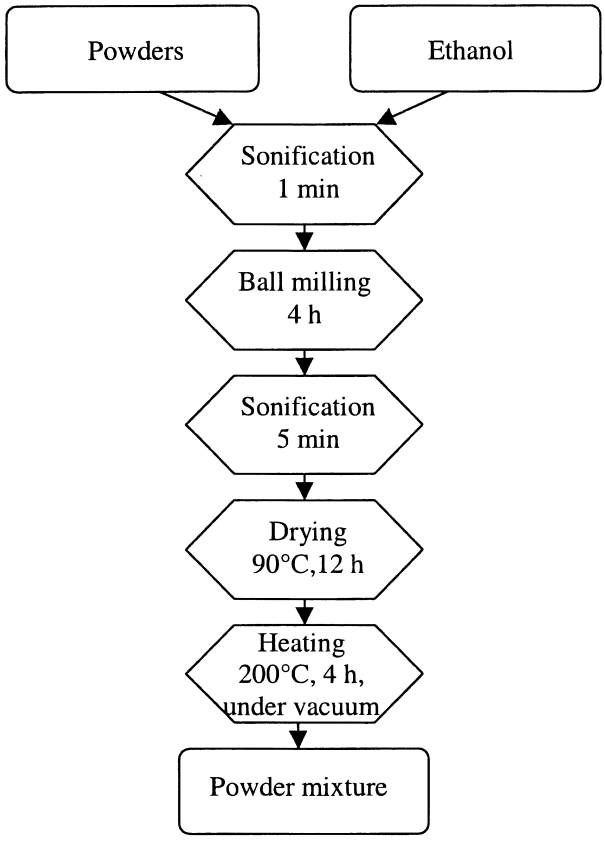

Fig. 1. Flow chart for the mixing of the powders.

Table 1
Elemental analysis of the SiCN powder

Elemental analysis (wt.%)				Atomic ratio
Si	C	N	O	C/N
58.3	6.5	34.6	0.6	0.2

Table 2
Characteristics of the sintering aids

Aids	d_{50}	Specific area (BET) m^2/g	Purity
Y_2O_3	1 μm	3.5	99.9
Al_2O_3	50 nm	48.4	99.9

Table 3
Elemental analysis of the SiCN nanocomposite material

Elemental analysis (wt%)					
Si	N	C	O	Al	Y
52.4	29.8	4.3	7.8	1.4	4.3

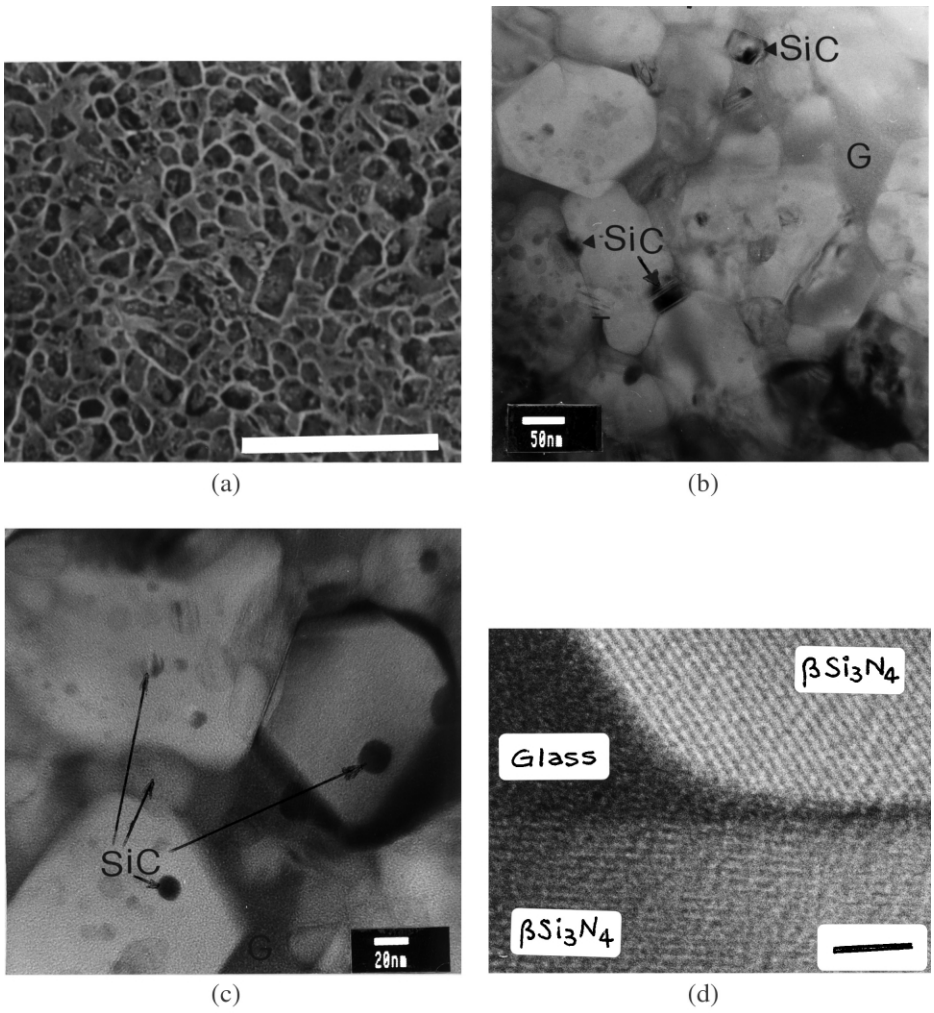

Fig. 2. Micrographs of the SiCN nanocomposite. (a) MEB micrograph: overview of the plasma etched material; bar = 1 μm; (b,c) TEM micrographs showing the quite equiaxed β-Si_3N_4 grains, the SiC spherical nanoparticles, the larger, twinned SiC particles in the grain boundaries and the YSiAlON glass pockets; bars: (b) = 50 nm, (c) = 20 nm; (d) TEM micrograph: glass pocket and thin intergranular film between two β-Si_3N_4 grains, bar = 5 nm.

between β-Si_3N_4 grains (Fig. 2b and c). Whose inside the Si_3N_4 grains were more numerous, whereas whose in between were bigger in size.

Using the results of the elemental analysis and under the assumption that the glass phase has a composition in the glass forming domain of the YSiAlON system, the proportions of the different phases were estimated. Based on the work by Lemercier et al.,[18] several mean atomic compositions were considered for the glass phase. The estimated quantity of glass ranged between 11 and 13 wt.%. The SiC content was about 5 and 2 wt.% of free carbon must be dissolved in the glass phase, that is consistent with the upper limit of solubility of carbon in oxycarbide glasses.[19]

2.2. Testing

Compressive creep tests were carried out in air environment using a dead load machine. The change in specimen length was monitored with a linear variable differential transformer (LVDT) and a chart recorder. The scatter of the measurement for the deformation was within 2 μm.

The specimens were parallelepipedic bars (3×3×7 mm^3). They were placed between two silicon carbide platens. The parts in contact with the specimen were coated with boron nitride to reduce friction between the sample and the fixtures. Under these operating conditions, very little barrelling of the samples was observed after testing. The furnace was allowed to stabilise for 45 min at the test temperature before applying the load.

As the tests were conducted under constant load instead of constant stress, as soon as deformation becomes noticeable, true strain (ε_t), true stress (σ_t) and true strain rate ($\dot{\varepsilon}_t$) were calculated from the engineering strain ($\varepsilon_e = [h - h_0/h_0]$), engineering stress ($\sigma_e$) and engineering rate ($\dot{\varepsilon}_e$), using the boundary condition of a constant volume during the deformation. For the frictionless case,[20]

which corresponds to no barrelling, the following expressions were used:

$$\varepsilon_t = \ln(1 + \varepsilon_e) \quad (1)$$

$$\sigma_t = (1 + \varepsilon_e)\sigma_e \quad (2)$$

$$\dot{\varepsilon}_t = \dot{\varepsilon}_e[1/(1 + \varepsilon_e)] \quad (3)$$

Although, in compression, ε_t, σ_t and $\dot{\varepsilon}_t$ are negative, their absolute values were considered in drawing the curves.

3. Experimental results for the as-sintered nanocomposite material

3.1. Creep data

Isobaric tests were carried out at constant temperature between 1150 and 1350°C under an initial applied stress of 90 MPa and isothermal tests at 1350°C under stresses ranging from 45 to 180 MPa. To assess the repeatability of the response of the material, the test at 1350°C under 90 MPa was duplicated, leading to a difference of 2% in strain (24.6 and 26.5%) after 50 h (see Fig. 5, full and open squares). The corresponding accuracy on the creep rate was 5%. True strain (%) against time data are showed in Figs. 3 and 4, respectively. Each test lasted 50 h with the exception of the experiment at 1350°C under 180 MPa when the sample broke after 33 h. However, after a heat-treatment for 5 h at 1600°C, the sample sustained successfully the 50 h duration under the same temperature and stress conditions. All the creep curves show a short primary stage followed by an pseudo-stationary stage. A tertiary stage, very short, was observed only for the sample that broke during the test.

In Fig. 5, the creep curve at 1350°C under 90 MPa is compared with those obtained under the same conditions in a previous work[21] for a monolithic silicon nitride hot-pressed for 2 h at 1550°C under 35 MPa with 6 wt.% Y_2O_3 and 3 wt.% Al_2O_3 as sintering aids and a SiC/Si_3N_4 composite elaborated from a mixture of 68.8 wt.% Si_3N_4 + 22.2 wt.% of the same SiCN nanoparticles and 6 wt.% Y_2O_3 + 3 wt.% Al_2O_3 by hot-pressing for 2 h at 1600°C. Whereas the addition of SiCN nanoparticles to Si_3N_4 powder (UBE SNE10 grade), leading to a micro-nano composite, resulted in an increase in the creep resistance, the present nanocomposite exhibits an enhanced ductility with the creep deformation being about three times that of the monolith. A stress 4 times smaller (45 instead of 180 MPa) was sufficient to obtain for the nanocomposite the same deformation than for the monolith.

Similarly, true strain rates versus time data are compared in Fig. 6. Open symbols correspond to true strain rates calculated from the actual applied stress which decreases as the deformation proceeds. Full ones and crosses correspond to the data corrected for a constant applied stress of 90 MPa using the stress exponents determined from the $\log\dot{\varepsilon}$ versus $\log\sigma$ diagrams. Whereas the change in cross section leads to negligible

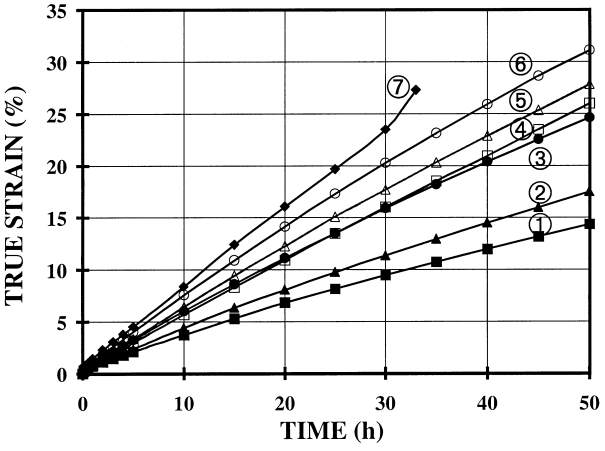

Fig. 4. Creep curves. Isothermal tests $T = 1350$°C. Nominal stresses: ①=45 MPa, ②=60 MPa, ③=90 MPa, ④=110 MPa, ⑤=135 MPa, ⑥=150 MPa, ⑦=180 MPa.

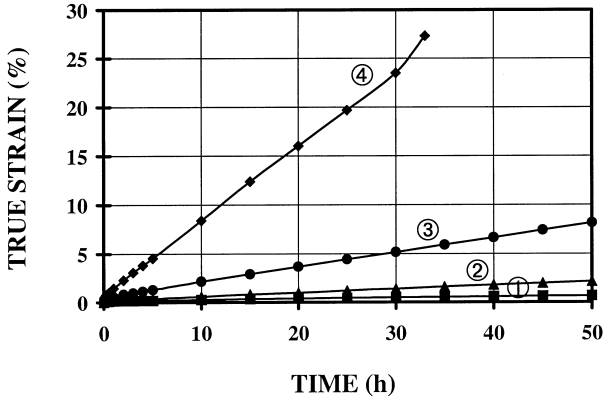

Fig. 3. Creep curves. Isobaric tests: $\sigma = 180$ MPa. ①=1200°C, ②=1250°C, ③=1300°C, ④=1350°C.

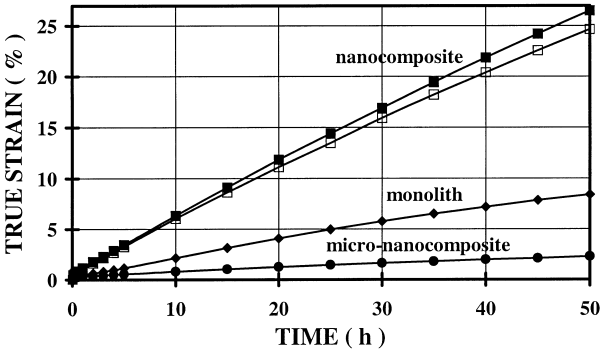

Fig. 5. Comparison of the creep curves at 1350°C under 90 MPa for the present nanocomposite ■ and □, the corresponding monolith ◆ and the SiC/Si_3N_4 composite ●.

correction for the micro-nanocomposite and the monolith, the correction becomes noticeable for the nanocomposite. The creep rate after 50 h increases from 8.5×10^{-8} s^{-1} for the micro-nanocomposite to 3.5×10^{-7} s^{-1} for the monolith and up to $1.23\pm0.05\times10^{-6}$ s^{-1} for the present nanocomposite. The maximum in creep rate observed around the 10th hour in the monolith was attributed to the α- to β-Si_3N_4 phase transformation.[21,22] For both the monolith and the micro-nanocomposite, the creep rate kept decreasing at the end of the tests, that is indicative of a microstructure not yet stabilised. In contrast, the creep rate corrected for constant stress shows that in the case of the nanocomposite a steady state creep is reached after a few hours.

3.2. Stress exponent and apparent activation enthalpy

The steady state creep rate was related to stress and temperature using the Dorn–Boltzmann relation:

$$\dot{\varepsilon} = Ad^{-p}\sigma^{n}\exp(-E_a/RT) \quad (4)$$

where A is a constant, d the mean grain size, p the grain size exponent, σ the stress, n the stress exponent, E_a the apparent activation enthalpy, R the gas constant and T the absolute temperature.

The true creep rates were measured in the stationary creep stage at a 30 h duration for nominal stresses of 45, 60, 90, 135, 150 and 180 MPa. Actual stresses, calculated according to Eq. (2), were used in the $\ln\dot{\varepsilon}$ vs. $\ln\sigma$ diagram (Fig. 7). The data showed a departure from linearity for stresses above 90 MPa. The linear fit for stresses from 45 to 90 MPa gives $n=0.95$ with a correlation factor of 0.972. It is worth noticing that the creep rate under 180 MPa nominal stress measured for a sample heat-treated 5 h at 1600°C is well aligned with the data of the low stress domain. At the moment, we have no explanation for the departure from linearity at high stresses. Further work is needed to elucidate this point.

The apparent activation enthalpy for creep deformation determined from the steady state creep rate against reciprocal temperature (Fig. 8) was found equal to 580 kJ/mol.

3.3. Microstructure and phase changes

At the end of the creep tests, the surface of the samples was black. SEM observations showed that the scale consists in acicular crystals, homogeneously distributed into an amorphous glaze. Cristoballite and β-$Y_2Si_2O_7$ were identified by XRD, that reveals a diffusion of yttrium toward the surface. The weight gain was very low, not measurable at 1350°C and less than 1% at 1400°C. The oxidised scale was very thin, irregular and discontinuous so that an attempt to measure its thickness by SEM on a cross-section of a sample crept for 50 h at

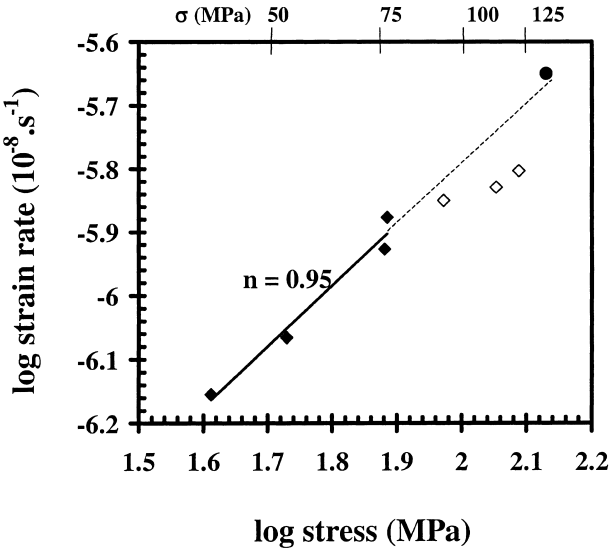

Fig. 7. True strain rate versus stress at 1350°C.

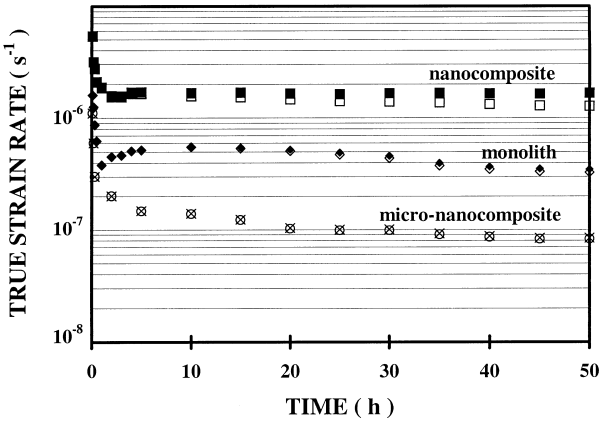

Fig. 6. True strain rate versus time at 1350°C under 90 MPa. Full symbols and crosses correspond to the data corrected for constant stress.

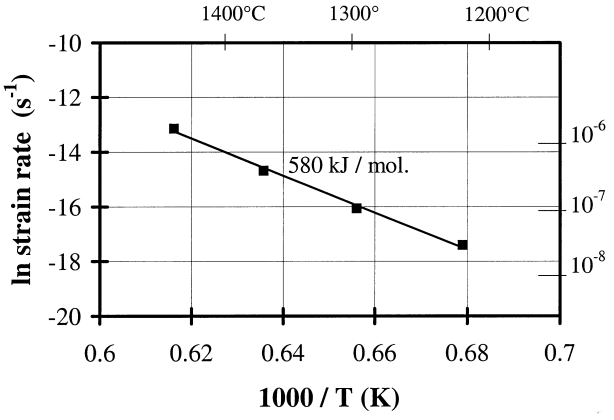

Fig. 8. True strain rate versus reciprocal absolute temperature.

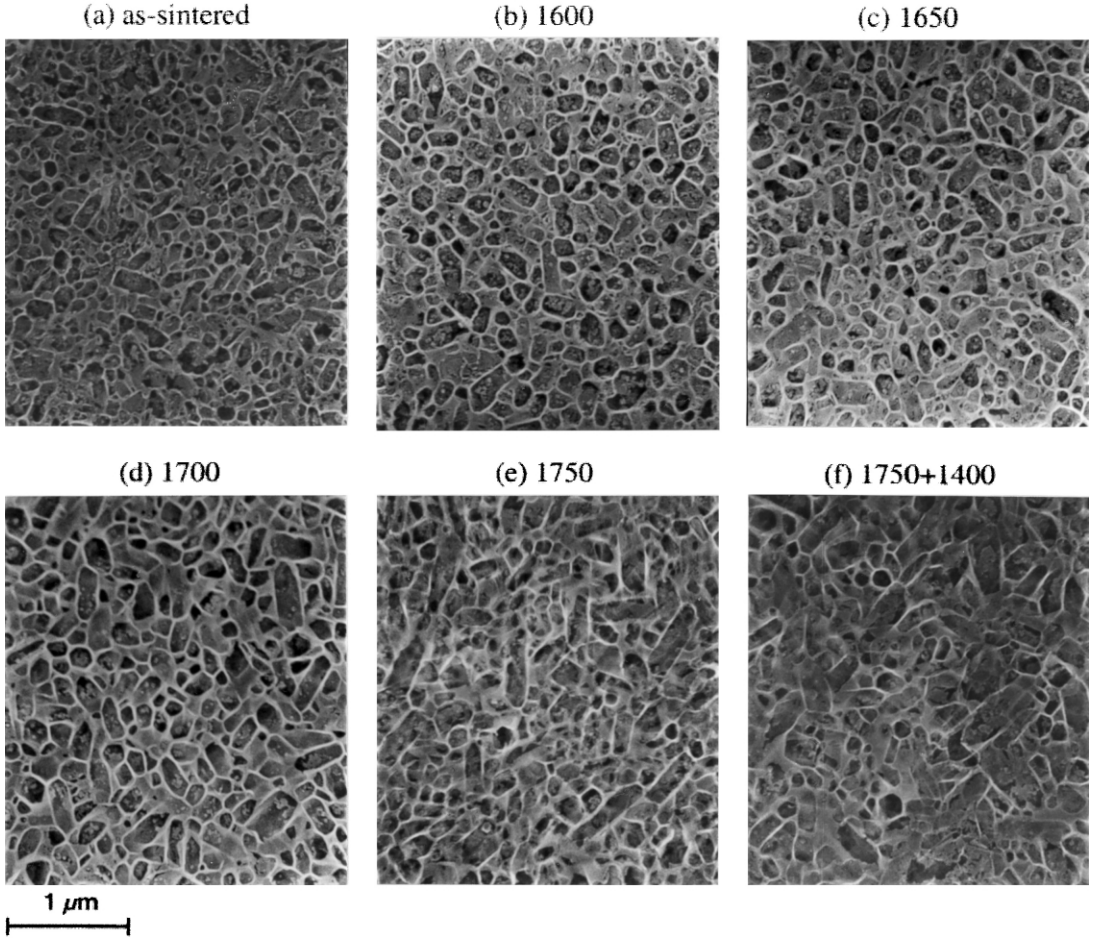

Fig. 9. (a) MEB micrographs of the as-sintered nanocomposite, (b) the material heat-treated at 1600°C, (c) 1650°C, (d) 1700°C, (e) 1750°C and (f) the two step heat-treated material .

1350°C was unsuccessful. So, the oxidation resistance of the nanocomposite is very good, even better than that of the micro-nanocomposite for which the oxidised scale was 15 μm under the same experimental conditions.

SEM investigations of cross-sections did not evidenced any significant change in the microstructure. However, X-ray diffraction studies revealed a slight crystallisation of the glassy secondary phase. The nature of the crystalline phases was difficult to assess. It must be β-$Y_2Si_2O_7$ and Al_2SiO_5, for these phases form during a heat-treatment at 1400°C, as will be seen in Section 4. No sign of cavitation was observed in the crept samples.

4. Influence of post-sintering heat-treatments

Post-sintering heat-treatments were performed in a graphite die under flowing nitrogen. The samples were embedded in a powder bed of silicon nitride to avoid decomposition.[23] The treatments lasted 5 h at 1600, 1650, 1700 and 1750°C. A heat-treatment for 3 h at 1400°C was also included during the cooling step of a 1750°C heat-treatment.

4.1. Microstructural observations

SEM micrographs of the heat-treated material are compared with the as-sintered material in Fig. 9. Whereas no change in the grain size and morphology is noticed after the 1600°C heat-treatment, a significant grain growth appears for heat-treatments at higher temperatures with the β-Si_3N_4 grains exhibiting a more and more acicular shape. The more elongated grains are about 500 nm in length and up to 800 nm after heat-treatment at 1700 and 1750°C respectively. TEM micrographs of a sample having experienced the two-step treatment at 1750 and 1400°C are showed in Fig. 10. The additional treatment at 1400°C did not lead to further grain growth. Most of the SiC nanoparticles are now incorporated into the β-Si_3N_4 grains (Fig. 10b). X-ray diffraction patterns show a partial crystallisation

(a)

(b)

Fig. 10. TEM micrographs of the nanocomposite heat-treated for 5 h at 1750°C and 3 h at 1400°C: (a) notice the acicular growth by comparison with Fig. 2b, bar = 100 nm; (b) SiC spherical nanoparticles incorporated in a β-Si_3N_4 grain, bar = 40 nm.

of the glassy intergranular phase into yttrium disilicate (β-$Y_2Si_2O_7$) and aluminium silicate (Al_2SiO_5).

4.2. Room temperature mechanical properties

Toughness and flexural strength at room temperature are collected in Table 4. The samples were parallelepipedic bars (25×4×3 mm^3; l, w, h). The tensile faces were polished to 3 μm finish and the tensile edges were chamfered. Polishing was very difficult owing to the high hardness (HV = 1600±50) and the small size of the grains. Grain pull-out could not be completely prevented. Toughness was determined by Vickers indentation method using Evans and Charles' equation:[24]

Table 4
Room temperature mechanical characteristics[a]

Heat treatment		Toughness	Strength
Temperature (°C)	Time (h)	(MPa $m^{1/2}$)	(MPa)
		3.6±0.3	470±30
1600	5	3.5±0.1	570±30
1650	5	3.8±0.5	
1700	5	4.6±0.4	
1750	5	5.4±0.4	
1750 + 1400	5 + 3	6.9±0.7	530±30

[a] The data were obtained from six measurements for the toughness and from four samples for the strength.

$$K_{1C} = 7.5 \times 10^{-8} \frac{P}{c^{3/2}} \quad (5)$$

where P is the indentation load (N) and $2c$ the radial crack length (m). The indentation load was 294 N in order that the condition leading to a "half penny" crack system, $c/a > 2.5$ (with $2a$ the hardness impression), be satisfied. The flexural strength was determined at a cross-head speed of 0.2 mm/min using a three-point bending jig with a 20 mm span.

Three-point bend flexural strength of the as-sintered material was rather low for a silicon nitride and the heat treatment increased it markedly (by 20%). The toughness remained unchanged after heat-treatment at 1600°C and increased gradually from 3.5 to 5.4 MPa $m^{1/2}$ for heat treatment at increasing temperatures. An additional increase was obtained after a further heat-treatment at 1400°C.

4.3. Change in creep resistance

The creep resistance of the heat-treated samples were compared to that of the as-sintered material at 1350°C under 180 MPa. The curves are reported in Fig. 11 and compared with the behaviour of the monolithic silicon nitride in Fig. 12.

As already mentioned in Section 3.1, the creep deformation increased after a 1600°C-heat treatment, reaching a true strain of 45% within 50 h. On the contrary, for heat treatment at higher temperatures, the creep resistance was improved. The higher the temperature of the heat-treatment, the higher the creep resistance. Including the crystallisation stage after the 1750°C treatment further enhanced the creep resistance that became similar to that of the monolith heat-treated at 1600°C for 5 h and to that of the micro-nanocomposite for which a treatment at 1750°C for 5 h had no influence.

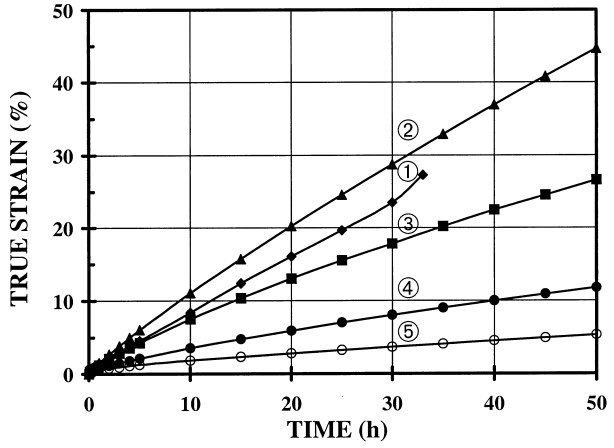

Fig. 11. Creep curves at 1350°C under 180 MPa: ① as-sintered, ②, ③ and ④ heat-treated at 1600, 1700 and 1750°C, ⑤ heat-treated 5 h at 1700°C and 3 h at 1400°C, respectively.

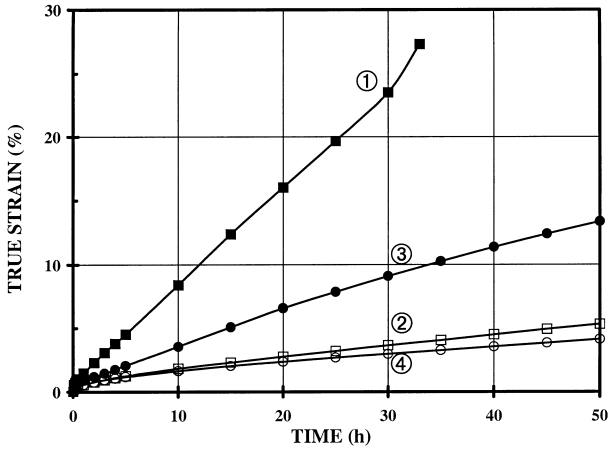

Fig. 12. Comparison of the creep curves of the SiCN nanocomposite and of the corresponding monolith at 1350°C under 180 MPa. Nanocomposite: ① as-sintered, ② heat-treated 5 h at 1750°C + 3 h at 1400°C; monolith: ③ as-sintered, ④ heat-treated 5 h at 1600°C.

5. Discussion

5.1. Creep mechanism

The overall behaviour of the as-sintered nanocomposite is similar to that of silicon nitride ceramics densified with similar amount of sintering aids, except for the quite low creep resistance. This latter point will be dealt with in next section. For these ceramics containing a noticeable amount of amorphous intergranular phase, the primary stage is dominated by the viscoelastic response of the glass phase which redistributes itself from high pressure regions to lower pressure regions.[25–27] Moreover, due to a macroscopic gradient that appears between the bulk and the surface, a fraction of the glass phase is exuded to the surface during the very first hours of the test.[28,29] Then, grain boundary sliding becomes restricted by grain-to-grain contacts at asperities. The increasing number of contacts as the width of the intergranular films becomes thinner entails a strain hardening effect resulting in a pseudo-stationary stage. A true steady-state creep is reached when the recovery effect due to diffusional creep compensates the strain hardening effect. So, the creep mechanism in the stationary stage is grain-boundary sliding accommodated by solution of β-Si_3N_4 into the glass phase at steps along boundaries, migration of the species through the glass and reprecipitation.[30]

The main feature of the present material is that the stationary stage, with a stress exponent equal to unity characteristic of a Newtonian diffusional creep, is reached in a very short time (5 h) compared to the case of the micro-nanocomposite (for which it requires about 30 h) and to the monolith. Two reasons can be put forward to explain the shortness of the transient regime: (i) the small grain size, that implies a large surface area of grain boundaries and consequently a thin thickness (~ 1 nm) of the intergranular films for a given amount of glass phase; and (ii) the remarkable stability of the microstructure (the α- to β-Si_3N_4 transformation is completed at the end of sintering, contrary to the cases of the monolith and the micro-nanocomposite, and grain growth does not occur at temperatures lower than 1600°C).

The apparent activation enthalpy for steady state creep, $E = 580$ kJ mol^{-1}, is similar to that determined for the micro-nanocomposite (590 kJ mol^{-1}) and significantly higher than that of the monolith (514 kJ mol^{-1}).[21] The solution-diffusion-reprecipitation mechanism consists in three sequencial steps, and assuming that the interface kinetics for solution and precipitation are the same, then, the mechanism may be controlled either by the solution of Si_3N_4 in the liquid (interface reaction) or by the matter transport (diffusion): the slower of the two will be rate controlling and the smaller activation energy would dominate at high temperature. In a study of the α- to β-Si_3N_4 transformation in connection with the densification of Si_3N_4 with MgO or Y_2O_3 additives, Hampshire and Jack[31] measured the same activation energy for the α- to β-Si_3N_4 transformation (405 kJ mol^{-1}), whatever the oxide. This value being close to the dissociation energy of the Si-N bond (435±38 kJ mol^{-1}), they concluded that the mechanism of the transformation was likely the same and required the breaking of Si–N bonds. Messier et al.[32] arrived at the same conclusion that the α- to β-Si_3N_4 transformation is a reconstructive transformation of second co-ordination that needs the presence of a liquid in which the less stable, more soluble phase (α) goes into solution and is precipitated as the less soluble, more stable form (β). Hence, this suggests that the activation enthalpy of the transformation is the same as the activation enthalpy for interface reaction, and is independent of the chemical composition of the liquid phase. On the contrary, the activation enthalpy for the diffusion step depends on the

viscosity of the amorphous phase which varies with the composition. So, Hampshire and Jack concluded that densification with MgO (425 kJ mol^{-1}) was controlled by the interface reaction whereas densification with Y_2O_3 (555 kJ mol^{-1}) was controlled by diffusion (i.e. the transition temperature between diffusion and interface reaction control was shifted to a temperature higher than the sintering temperature). For the present material and the material studied in Ref. 21, the activation enthalpies are superior to the activation enthalpy for interface reaction so that the transport of matter is likely to be the limiting step. Since the starting compositions for the composites were chosen to lead to the same theoretical SiC content, it may be assumed that the SiC containing grades have a glass phase with about the same chemical composition and consequently the same activation enthalpy. The glass transition temperature of the intergranular phase can be evaluated through the change in slope when measuring the evolution of Young's modulus with temperature.[33] In Ref. 21, it was showed that the SiC micro-nanocomposite has a T_g higher by about 75°C than that of the monolith. The resulting higher viscosity at a given temperature was supposed to be associated with the presence of carbon in the glass phase. This is supported by the conclusion that about 2 wt.% free carbon must be dissolved in the glass phase (Section 2.1). Carbon that may have the ability to bond four silicon ions in the glass network provides a still more tightly cross-linked structure than found in oxynitride glasses and enhances the properties to a much more extent,[34] that can explain the higher activation enthalpies of the composites compared to the monolith.

5.2. Creep resistance

Since stress exponents and activation enthalpies are the same for the two composites, their different creep resistance must come from their microstructures that differ in the SiC particle distribution and in the Si_3N_4 grain size. The high creep resistance of the micro-nanocomposite was explained by the fact that the SiC particles were mainly in the intergranular phase, obstructing the easy path for diffusion, or gathered in glass pockets, trapping a large amount of glass. On the contrary, no SiC clusters were observed in the nanocomposite where the SiC particles were in majority inside the Si_3N_4 grains. Furthermore, the Si_3N_4 grain size is smaller in the nanocomposite. So, the creep resistance of the nanocomposite is ten times less than that of the micro-nanocomposite. The very fine, quasi equiaxed microstructure of the nanocomposite (mean grain size $\sim$ 150 nm) is the reason why it shows a creep deformation even greater than that of the monolith (mean grain size $\sim$250–300 nm).

The improvement in creep resistance after heat treatments at $T \geqslant 1700$°C is due to an increase in grain size and, above all, to the development of the β-Si_3N_4 acicular morphology (Fig. 10d and e). This change from equiaxed to acicular shape induces also an increase in the toughness at room temperature, resulting from energy dissipating mechanisms such as crack-deflection, crack-bridging and grain pull-out[35] as showed for Si_3N_4–SiC whisker composites[36] and self-reinforced silicon nitride.[37] The additional treatment at 1400°C, that induces a partial crystallisation of the glass phase leading to a further increase in toughness, reduces the creep deformation by reducing the quantity of liquid phase and changing its chemical composition which, through the formation of silicates, is enriched in nitrogen, that enhances its viscosity.

6. Conclusion

This silicon nitride based nanocomposite fabricated from nanosized SiCN powder and $Al_2O_3 + Y_2O_3$ densification aids has showed a high creep deformation at 1350°C due to its fine equiaxed microstructure that remained stable even after a heat treatment for 4 h at 1600°C.

From the value of the stress exponent ($n = 1$) and that of the apparent activation enthalpy (580 kJ mol^{-1}), it has been showed that the creep behaviour was governed by grain boundary sliding accommodated by dissolution of Si_3N_4 in the amorphous intergranular phase, diffusion through the glass and reprecipitation, diffusion being the rate controlling step.[30] As it has been demonstrated[9] that the monolithic silicon nitride can be tailored to exhibit a very high ductility ($\varepsilon = 85\%$ in tension at 1580°C under a true strain rate of 2.5×10^{-5} s^{-1}), it is anticipated that this material, that presents a creep rate 4 times higher than that of the monolith, should behave superplastically at a lower temperature and/or a higher strain rate.

Moreover, post-sintering heat treatments allowed the development of an acicular microstructure and a partial crystallisation of the amorphous phase leading to a considerable improvement of the creep resistance. Therefore, this Si_3N_4/SiC nanocomposite is a promising grade since its high ductility in the as-sintered state, allowing net-shaping by hot-forging, can be easily converted into a high creep resistance by heat treatment after the shaping stage.

Acknowledgements

This work was supported by the CNRS in the frame of the GDR 1168 'Poudres céramiques monophasiques à base de silicium'. Additional financial support was provided by DGA, Ministry of Defence. The SiCN powder was fabricated in the Centre d'Etudes Nucléaires

de Saclay (France). The authors wish to thank S. Baud and Dr. F. Thévenot of ENSM in Saint Etienne (France) for the plasma etching and B. Soulestin (SPCTS, Limoges) for his assistance in the preparation and observation of the TEM samples.

References

1. Wakai, F., Kodama, Y., Sakaguchi, S., Murayama, N., Izaki, K. and Niihara, K., A superplastic covalent crystal composite. *Nature*, 1990, **344**, 421–423.
2. Rouxel, T., Wakai, F. and Izaki, K., Tensile ductility of superplastic $Al_2O_3-Y_2O_3-Si_3N_4$/SiC composites. *J. Am. Ceram. Soc.*, 1992, **75**, 2363–2372.
3. Chen, I. W. and Hwang, S. L., Shear thickening creep in superplastic silicon nitride. *J. Am. Ceram. Soc.*, 1992, **75**, 1073–1079.
4. Wu, X. and Chen, I. W., Exaggerated texture and grain growth in a superplastic SiAlON. *J. Am. Ceram. Soc.*, 1992, **75**, 2363–2372.
5. Chen, I. W. and Hwang, S. L., Superplastic forming of SiAlON ceramics. *J. Am. Ceram. Soc.*, 1994, **77**, 2575–2585.
6. Rossignol, F., Rouxel, T., Besson, J-L., Goursat, P. and Lespade, P., Superplasticity in silicon nitride through the α to β phase transformation. *J. Phys. III France*, 1995, **5**, 127–134.
7. Kondo, N., Wakai, F., Nishioka, T. and Yamakawa, A., Superplastic Si_3N_4 ceramics consisting of rod-shaped grains. *J. Mater. Sci. Lett.*, 1995, **14**, 1369–1371.
8. Descamps, P., Beugnies, D. and Cambier, F., A two-step method to obtain superplastic silicon nitride with high thermomechanical properties. *J. Eur. Ceram. Soc.*, 1997, **17**, 433–437.
9. Rouxel, T., Rossignol, F., Besson, J-L. and Goursat, P., Superplastic forming of an α-phase rich silicon nitride. *J. Mater. Res.*, 1997, **12**, 480–492.
10. Burger, P., Duclos, R. and Crampon, J., Microstructure characterization in superplastically deformed silicon nitride. *J. Am. Ceram. Soc.*, 1997, **80**, 879–885.
11. Wang, C. M., Mitomo, M., Nishimura, T. and Bando, Y., Grain boundary film thickness in superplastically deformed silicon nitride. *J. Am. Ceram. Soc.*, 1997, **80**, 1213–1221.
12. Rosenflanz, A. and Chen, I. W., Classical superplasticity of SiAlON ceramics. *J. Am. Ceram. Soc.*, 1997, **80**, 1341–1352.
13. Kondo, N., Suzuki, Y. and Ohji, T., Superplastic sinter-forging of silicon nitride with anisotropic microstructure formation. *J. Am. Ceram. Soc.*, 1999, **82**, 1067–1069.
14. Kondo, N., Ohji, T., Suzuki, Y. and Nagano, T., Effect of α-phase on superplastic behavior of silicon nitride. *J. Ceram. Soc. Japan*, 1999, **107**, 388–390.
15. Luce, M., Croix, O., Robert, C. and Cauchetier, M., Laser synthesis of ultrafine Si/C/N composite powders. In *Ceramic Powder Sc., III*, ed. G. L. Messing, S. I. Hihane and H. Hausner. Ceramic Trans. Vol. 12. The American Ceramic Society, Westerville, OH, 1990, pp. 267–274.
16. Cauchetier, M., Croix, O., Luce, M., Baraton, M. I., Merle, T. and Quintard, P., Nanometric Si/C/N composite powders: laser synthesis and IR characterization. *J. Eur. Ceram. Soc.*, 1991, **8**, 215–219.
17. Mayne, M., Bahloul-Hourlier, D., Doucey, B., Goursat, P., Cauchetier, M. and Herlin, N., Thermal behaviour of SiCN nanopowders issued from laser pyrolysis. *J. Eur. Ceram. Soc.*, 1998, **18**, 1187–1194.
18. Lemercier, H., Rouxel, T., Fargeot, D., Besson, J-L. and Piriou, B., Yttrium SiAlON glasses: structure and mechanical properties — elasticity and viscosity. *J. Non-Cryst. Solids*, 1996, **201**, 128–145.
19. Ramesh, R., Chevaux, P., Lemercier, H., Pomeroy, M. J. and Hampshire, S., Characterisation of oxycarbide glasses prepared by melt solidification. In *Euro-Ceramics V*. Key Engineering Materials, Vols 132–136, ed. D. Bortzmeter, M. Boussuge, Th. Fantozzi, G. Fantozzi, G. Lozes and A. Rousset. Trans. Tech. Publications, Uetikon-Zuerich, Switzerland, 1997, pp. 189–192.
20. Debschütz, K. D., Caspers, B., Schneider, G. A. and Petzow, G., Critical evaluation of the compressive creep test. *J. Am. Ceram. Soc.*, 1993, **76**, 2468–2474.
21. Besson, J-L., Mayne, M., Balhoul-Hourlier, D. and Goursat, P., Si3N4/SiC nanocomposites : influence of SiC nanoprecipitates on the creep behaviour. *J. Eur. Ceram. Soc.*, 1998, **18**, 1893–1904.
22. Besson, J-L., Rouxel, T. and Goursat, P., Ductility and creep resistance of a silicon nitride ceramic. *Scripta Materialia*, 1998, **39**, 1339–1343.
23. Chartier, T., Besson, J.-L., Goursat, P. and Mustel, W. Post-sintering heat treatments and creep of Si–Y–Al–O–N ceramics. In *Science of Ceramics 13*. Journal de Physique Colloque C1 Vol. 47, ed P. Odier, F. Cabannes and B. Cales. Les Editions de Physique, Courtaboeuf, 91944 Les Ullis, France, 1986, pp.673–678.
24. Evans, A. G. and Charles, E. A., Fracture toughness determination by indentation. *J. Am. Ceram. Soc.*, 1976, **59**, 371–372.
25. Lange, F. F., Clarke, D. R. and Davis, B. I., Compressive creep of Si_3N_4/MgO alloys. Part 2 Source of viscoelastic effect. *J. Mater. Sci.*, 1980, **15**, 611–615.
26. Arons, R. M. and Tien, J. K., Creep and strain recovery in hot-pressed silicon nitride. *J. Mater. Sci.*, 1980, **15**, 2046–2058.
27. Jin, Q., Ning, X. G., Wilkinson, D. S. and Weatherly, G. C., Redistribution of a grain-boundary glass phase during creep of silicon nitride ceramics. *J. Am. Ceram. Soc.*, 1997, **80**, 685–691.
28. Clarke, D. R., High temperature deformation of a polycrystalline alumina containing a glass phase. *J. Mater. Sci.*, 1985, **20**, 1321–1332.
29. Besson, J-L., Streicher, E., Chartier, T. and Goursat, P., Viscoelastic creep of nitrogen ceramics. *J. Mater. Sci. Lett.*, 1986, **5**, 803–805.
30. Wakai, F., Step model of solution–precipitation creep. *Acta Metall. Mater.*, 1994, **42**, 1163–1172.
31. Hampshire, S. and Jack, K. H., The kinetics of densification and phase transformation of nitrogen ceramics. In *Special Ceramics 7*. Proceedings of the British Ceramic Society, Vol. 31, ed D. Taylor and P. Popper. The British Ceramic Society, Stoke on Trent, UK, 1981, pp. 37–49.
32. Messier, D. R., Riley, F. L. and Brook, R. J., The α/β silicon nitride phase transformation. *J. Mater. Sci.*, 1978, **13**, 1199–1205.
33. Rouxel, T., Besson, J-L., Gault, C., Goursat, P., Leigh, M. and Hampshire, S., Viscosity and Young's modulus of an oxynitride glass. *J. Mater. Sci. Lett.*, 1987, **8**, 1158–1160.
34. Homeny, J., Nelson, G. G., Paulik, S. W. and Risbud, S. H., Comparison of the properties of oxycarbide and oxynitride glasses. *J. Am. Ceram. Soc.*, 1987, **70**, C114–116.
35. Rice, R. W., Ceramic matrix composite toughning mechanisms: an update. *Ceram. Eng. Sci. Proc*, 1985, **6**(7-8), 589–607.
36. Champion, E., Goursat, P., Besson, J-L., Madigou, V., Monthioux, M. and Lespade, P., Microstructure, strength and toughness of Si_3N_4–SiC whisker composites. *Ceram. Eng. Sci. Proc*, 1992, **13**(9–10), 732–739.
37. Becher, P. F., Lin H. T., Hwang, S. L., Hoffmann, M. J. and Chen I. W., The influence of microstructure on the mechanical behaviour of silicon nitride ceramics. In *Silicon Nitride Ceramics — Scientific and Technological Advances*, ed. I. W. Chen, P. F. Becher, M. Mitomo, G. Petzow and T. S. Yen. Materials Research Society, Pittsburgh, 1993, pp.147–158.